Materials Today Advances 22 (2024) 100493

Contents lists available at ScienceDirect

Materials Today Advances

journal homepage: www.journals.elsevier.com/materials-today-advances/

Enabling high-fidelity personalised pharmaceutical tablets through multimaterial inkjet 3D printing with a water-soluble excipient

Geoffrey Rivers [a], Anna Lion [a], Nur Rofiqoh Eviana Putri [a], Graham A. Rance [c], Cara Moloney [d], Vincenzo Taresco [e], Valentina Cuzzucoli Crucitti [a], Hannah Constantin [a], Maria Inês Evangelista Barreiros [a], Laura Ruiz Cantu [a], Christopher J. Tuck [a], Felicity R.A. J. Rose [b], Richard J.M. Hague [a], Clive J. Roberts [g], Lyudmila Turyanska [a], Ricky D. Wildman [a,**], Yinfeng He [a,f,*]

[a] Faculty of Engineering, University of Nottingham, NG7 2RD, UK
[b] Nottingham Biodiscovery Institute, School of Pharmacy, University of Nottingham, NG7 2RD, UK
[c] Nanoscale and Microscale Research Centre, University of Nottingham, NG7 2RD, UK
[d] School of Medicine, University of Nottingham, NG7 2RD, UK
[e] School of Chemistry, University of Nottingham, NG7 2RD, UK
[f] Nottingham Ningbo China Beacons of Excellence Research and Innovation Institute, University of Nottingham Ningbo China, Ningbo, China
[g] School of Life Sciences, University of Nottingham, NG7 2UH, UK

ARTICLE INFO

Keywords:
Multi-material printing
Water soluble
Drug delivery
Controlled release
Polypills

ABSTRACT

Additive manufacturing offers manufacture of personalised pharmaceutical tablets through design freedoms and material deposition control at an individual voxel level. This control goes beyond geometry and materials choices: inkjet based 3D printing enables the precise deposition (10–80 μm) of multiple materials, which permits integration of precise doses with tailored release rates; in the meanwhile, this technique has demonstrated its capability of high-volume personalised production. In this paper we demonstrate how two dissimilar materials, one water soluble and one insoluble, can be co-printed within a design envelope to dial up a range of release rates including slow (0.98 ± 0.04 mg/min), fast (4.07 ± 0.25 mg/min) and multi-stepped (2.17 ± 0.04 mg/min then 0.70 ± 0.13 mg/min) dissolution curves. To achieve this, we adopted poly-4-acryloylmorpholine (poly-ACMO) as a new photocurable water-soluble carrier and demonstrated its contemporaneous deposition with an insoluble monomer. The water soluble ACMO formulation with aspirin incorporated was successfully printed and cured under UV light and a wide variety of shapes with material distributions that control drug elution was successfully fabricated by inkjet based 3D printing technique, suggesting its viability as a future personalised solid dosage form fabrication routine.

1. Introduction

The advent of personalised medicines represents a promising frontier in patient treatment, requiring the manufacture of customized pharmaceutical dosage forms and devices [1–3]. Additive manufacturing (AM) (also known as 3D printing) can enable the fabrication of tailored structures [4–6]. The recent studies have shown that AM can be used to fabricate customised doses with bespoke release profiles of one pharmaceutical agent or multiple agents [7–10]. To date, AM of pharmaceuticals has utilised a variety of 3D printing modalities, including paste extrusion, digital light processing, binder jetting technologies, and laser sintering (LS) [11], and the design potential [12,13] achievable by these AM modalities. Recent advances in Multi-Material Ink-Jet 3D Printing (MM-IJ3DP) offer a promising route for precise, contemporaneous deposition of multiple materials at production scale [14,15], enabling intricate designs [16,17] with high fidelity and higher throughput than other AM techniques. However, the constraints imposed by MM-IJ3DP [14] present challenges, such as low viscosity of the feedstock materials, material stability, solidification speed and limitations on incorporation of particulate solids, which requires additional in-process

* Corresponding author. Faculty of Engineering, University of Nottingham, NG7 2RD, UK.
** Corresponding author.
E-mail addresses: ricky.wildman@nottingham.ac.uk (R.D. Wildman), yinfeng.he@nottingham.ac.uk (Y. He).

https://doi.org/10.1016/j.mtadv.2024.100493
Received 16 February 2024; Received in revised form 19 April 2024; Accepted 24 April 2024
Available online 14 May 2024

elements [18].

Owing to the limited choice of processable materials, existing MM-IJ3DP studies in personalised pharmaceutical tablets focus on drug delivery through swelling [19] and diffusion mechanisms [20]. The choice of excipients includes synthetic polymeric [21] and plant-based excipients [22,23], as well as co-excipients [24,25]. These release mechanisms limit the possibility for timed release of the active material and for desired modulation of release rates, which are required for the development of the next generation of personalised medicines; for this, a dissolution-mode release would be preferred. Of particular interest are biocompatible water-soluble polymers as excipients [26–28] such as poly-4-acrylomorpholine (poly-ACMO) which has been recently explored to produce gels [29], but not as a water soluble excipient. Achieving such controlled release with scalable AM process like MM-IJ3DP is relevant not only for human healthcare but also within veterinary [30,31] and environmental sciences [32,33] applications. However, formulations of water-soluble biocompatible materials for MM-IJ3DP are yet to be achieved, and the correlation between multi-material design and release rates is yet to be established.

In this paper we report on MM-IJ3DP of personalised pharmaceutical tablets through development of novel water-soluble inks that can enable tailoring of drug release profiles by geometrical design and co-printing with soft insoluble structures. The water-soluble formulation is based on photo-polymerisable acrylomorpholine (ACMO), whose polymer form acts as a model excipient to enable drug release in MM-IJ3DP tablets, exhibiting reliable printability, fidelity, medically relevant drug-loading capacity (demonstrated here with aspirin) and ability to attain a high molecular weight upon polymerization as needed for biocompatibility. These properties allow for a high degree of morphological control in MM-IJ3DP soluble structures compatible with mammalian cells. The release rate of therapeutic agents is determined by the surface area, which can be controlled by geometrical design, as we illustrate with tablets with different shapes, and with multimaterial structures. We demonstrate the feasibility of fabricating multi-drug tablets, so called 'polypills', with the drug release and dosage timing of individual active materials controlled by geometrical design. Moreover, exploiting the digital scalability of MM-IJ3DP, different designs with tailored release profiles can be manufactured contemporaneously in a single production batch (56 pills), which is essential for the manufacturing of personalised medicines.

2. Result and discussion

We propose that MM-IJ3DP, as a scalable AM process, can offer unprecedented opportunities for accessing personalised drug delivery compositions, and consequently drug release profiles, that are not feasible with conventional manufacturing methods, such as granulation, or direct compression. Therefore, we explored the possibility of manufacturing complex multi-material structures, exemplifying the range of designs available via inkjet based 3D printing, and manufacture multi-material structures with controlled release of a model drug. We exploited a pill design that changes the exposed soluble excipient surface to volume ratio over time to control drug release. MM-IJ3DP was used to produce a range of designs containing insoluble and soluble polymers (Fig. 1), in a single manufacturing step. The insoluble polymer part of the structure is designed to inhibit the ingress of a media and consequent drug elution, whilst the soluble part allows for release of the active material. The cross-linked and insoluble polymer was composed of a copolymer in a 25:75 wt/wt ratio of tricyclo[5.2.1.0 2,6]decanedimethanol diacrylate (TCDMDA) and ethylene glycol dicylcopentenyl ether acrylate (EGDPEA); the soluble parts of the structures were composed of poly-4-acryloylmorpholine (poly-ACMO). 2,4 diethyl-9H-thioxanthen-9-one (DETX) were used as the photoinitiator and ethyl 4-(dimethylamino) benzoate (EDB) as the accelerator to form a type II photoinitiation system for printing in ambient conditions (Fig. 1 and Supplementary Information SI1).

To demonstrate the increased complexity achievable through MM-IJ3DP, we produced composite cylindrical structures (outer diameter, d_o = 8 mm) with six designs (Fig. 1c): (1) a disc; (2) an annulus; (3) a non-soluble annulus with a water soluble core; (4) a water soluble annulus and insoluble core; (5) encapsulation of insoluble cubes (600 μm side length) by the soluble matrix; (6) and its inverse – encapsulation of soluble cubes by the insoluble matrix. In each case we were able to observe that the soluble component dissolved, leaving the insoluble component remaining (Fig. 1c).

In these structures, the surface area is varied to modify the time-dependent release rates. We measured the dissolution from geometries that included discs, squares, hexagons, pentagons, pentagrams and four-pointed stars with 2 mm thickness (Fig. 2a, see Methods). The dissolution rate (Fig. 2a) increased linearly with increasing surface area (R^2 = 0.9915), as expected from the classical Noyes–Whitney equation, showing that dissolution in this case is governed by the available contact area between ACMO and the dissolution media [34,35]. This result meant that we were able to design structures where the dynamic contact surface area of the soluble part can be used to control the release rates – i.e., a variable surface area for contact with the solvent, as ACMO is dissolved, can be designed *a priori*. This approach to dosage form manufacture demonstrates how, through manipulation of the combination of soluble and non-soluble materials, it may be possible to control the release of any API in a temporal and 'digitised' manner that is not achievable by more currently used manufacturing methods.

The suitability of poly-ACMO as a model excipient from a bio-safety perspective starts from cell viability assays. Mouse 3T3 fibroblasts were exposed to poly-ACMO, released from printed structures, with different concentrations from 0.001 % to 1 wt% for a period of up to 24 h (Fig. 2b). According to the Food and Drug Administration (FDA) [36], an excipient is deemed non-toxic if it has no significant effect on cell viability following 6 h exposure [37]. No evidence of cytotoxicity was

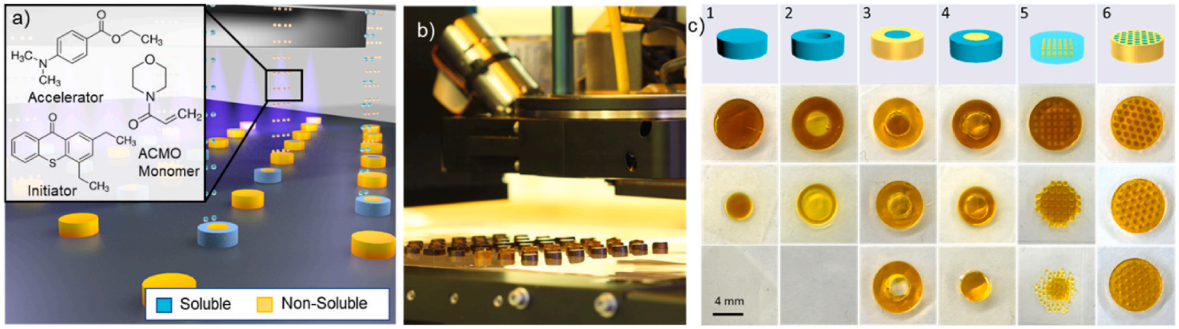

Fig. 1. a) Schematic illustration of multi-material inkjet-based 3D printing MM-IJ3DP and chemical structures of the soluble ink components (inset); **b)** Photograph of printed multi-material, MM-IJ3DP produced designs printed in a single batch **c)** Schematics of designs (top row) and corresponding photographs of MM-IJ3DP printed cylindrical structures as printed (second row), after partial (third row) and full (bottom row) dissolution of the soluble material.

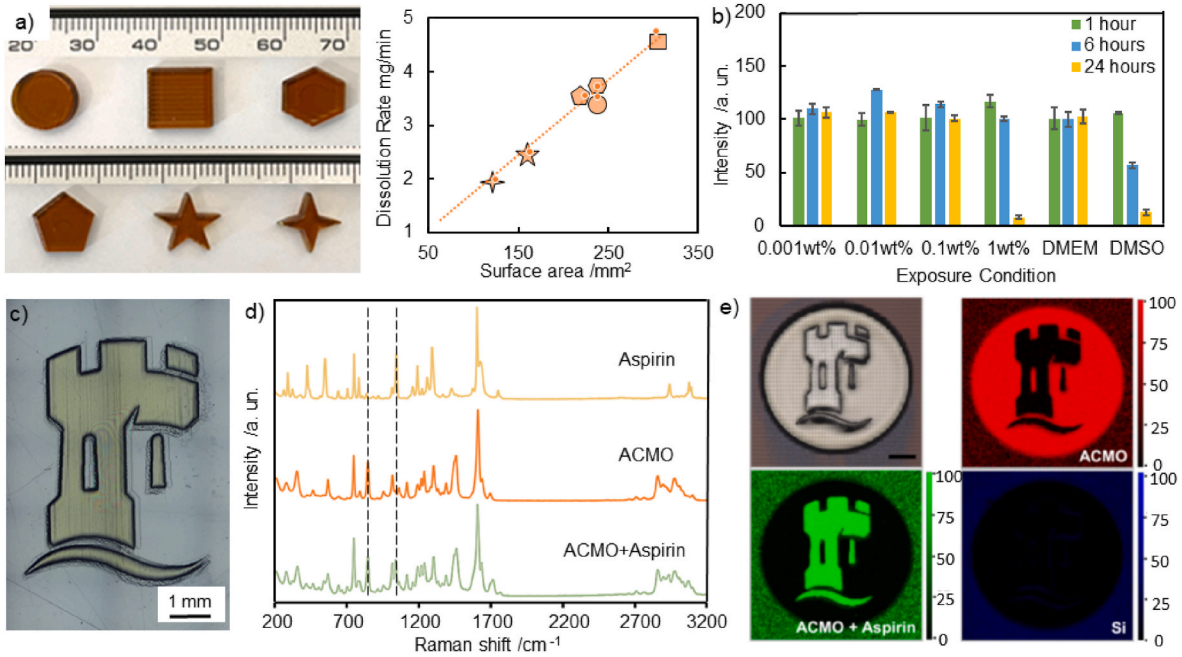

Fig. 2. **a)** A photograph of printed poly-ACMO structures and the dependence of dissolution time on the surface area of these structures. **b)** Cell viability of 3T3 fibroblast cells following 1 h, 6 h and 24 h exposure to poly-ACMO solution with different weight concentrations. Error bars represent mean ± standard deviation for $n = 4$ independent repeats. **c)** Photograph of the University of Nottingham logo printed with 30 wt% aspirin ACMO ink. Black outline indicates designed geometry. **d)** Representative Raman spectra of aspirin, poly-ACMO and 30 wt% aspirin poly-ACMO (top to bottom). **e)** Optical micrograph and confocal Raman mapping images of poly-ACMO (red), poly-ACMO with aspirin (green) and silicon substrate (blue). Scale bar is 1 mm.

observed in our experiments following 6 h exposure at all the concentrations studied. Reduced cell viability was observed after 24 h exposure to 1 wt% poly-ACMO only. At this concentration we observed some precipitation of poly-ACMO over time, which is a likely reason for the observed reduced viability.

Having established the utility of MM-IJ3DP for the manufacture of complex composites and confirmed the linear dependence of dissolution on surface area, we included an API into the soluble material. ACMO-only and ACMO-aspirin (30 wt%) inks were formulated, and co-printed into a pill (outer diameter, d = 5 mm, h = 1 mm) with the asprin loaded region embedded in the centre of the pill (within the 'castle') (Fig. 2e top-left). Raman spectroscopy analysis revealed characteristic peaks for aspirin and ACMO (1039 and 846 cm^{-1}, respectively), confirming successful incorporation and controlled distribution of aspirin (Fig. 2d and e). The printing strategy was that in every layer, the inks were deposited sequentially with the UV dose applied in between to prevent/minimize cross-contamination. No indication of intermixing between the inks at the interfaces was observed (Fig. 2e). To quantify the aspirin loading of the printed pill, the structure was dissolved in deuterated chloroform for subsequent analysis by ^{1}H NMR spectroscopy. After dissolution, a total aspirin loading was calculated to be 6.9 ± 0.3 wt% from the whole pill, comparable to the expected value for this design (6.4 wt%) and within typical pharmaceutical quality standards [38]. For printed 30 wt% aspirin poly-ACMO, only ~ 1 mol% of acrylate residues were found (Supplementary Information, SI2), indicating that the presence of aspirin does not interfere with the polymerization process.

Differential Scanning Calorimetry (DSC) data (Fig. 3a) and polarized optical microscopy (PLM) studies (Supplementary Information, SI2) revealed that aspirin retained an amorphous physical state in printed poly-ACMO with aspirin. Further studies using X-ray diffraction (XRD) confirmed that aspirin did not recrystallize after ink curing (Fig. 3b). We

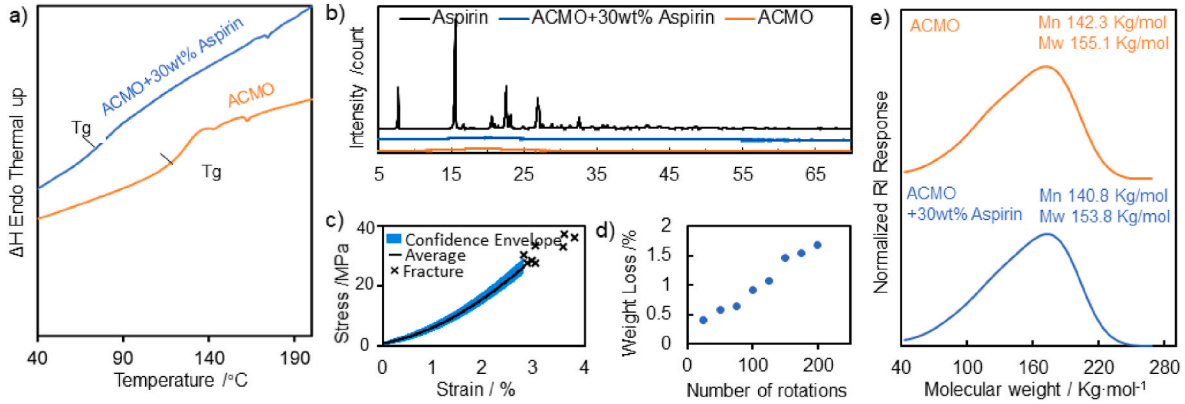

Fig. 3. **a)** DSC measurements of poly-ACMO without and with 30 wt% aspirin loading, indicating *Tg* values, and **b)** corresponding X-ray diffraction patterns tracking the presence of crystallization within the pill. **c)** Compression test of the poly-ACMO pill, with error envelope representing 95 % confidence interval, $n = 8$. **d)** Friability of the poly-ACMO pill. **e)** Molecular weight evaluation using GPC in aqueous column for printed poly-ACMO without and with 30 wt% aspirin loading.

propose that interactions, such as hydrogen bonding between the ACMO, poly-ACMO and aspirin, as observed from the shift of characteristic peaks in the ^{1}H NMR spectra, hindered recrystallization (Supplementary Information, SI2).

To check that the printed dosage forms could meet standard physical tablet criteria, strength and friability tests were performed. The fracture strength of printed poly-ACMO was found to be 32.0 ± 4.3 MPa (assessed using tablets $d = 8$ mm, $h = 3$ mm; Fig. 3c) and the friability weight loss was less than 1 % after 100 cycles (assessed using cubes with 3 mm sides; Fig. 3d), both values meeting the production requirements of the US pharmacopeia (USP). The molecular weight of MM-IJ3DP printed poly-ACMO was characterized by GPC (Fig. 3e), determining that the M_n and M_w were 142,300 and 155,100 g/mol, respectively. Aspirin-loaded poly-ACMO pills showed comparable molecular weight (M_n 140,800 g/mol, M_w 153,800 g/mol), hence confirming that any potential interaction between the aspirin and ACMO did not significantly affect in-print polymerization. The dispersity ($Đ = M_w/M_n$) for the poly-ACMO and aspirin loaded poly-ACMO was 1.10, both of which are within the range indicative of a narrow molecular size distribution and controlled polymerization (1.02–1.10) during IJ3DP [39,40]. The printed tablets have a shelf life of at least one month if sealed and stored in a dry environment. Under exposure to ambient conditions, the tablets remain stable for up to one week, after which macroscopic cracks appeared due to moisture absorption.

The successful demonstration of MM-IJ3DP solid dosage forms was used for designing tablets with release profiles that varied by virtue of control of the spatial variation of the soluble component alone. Four cylindrical multi-material designs were printed with standard tablet sizes ($d = 8$ mm, $h = 3$ mm) using a combination of the insoluble ink and the soluble poly-ACMO with aspirin (Fig. 4a). Design 1: a standard cylindrical tablet, with a small core of crosslinked and insoluble polymer. Design 2: a capped cylindrical tablet with top and bottom impermeable surfaces, designed to have a reduced dissolution rate compared to Design 1. Design 3: a capped and partially walled cylindrical tablet with the partial wall placed at the outer radius (R), designed to reduce the surface area normal to the radial direction. Design 4: a capped and partially walled cylindrical tablet with the partial wall placed at a radial location corresponding to $4R/3$, designed to have an initially rapid dissolution followed by a reduced dissolution rate. We note that after dissolution of the poly-ACMO parts of these designs, the insoluble components remained intact and retained their original geometrical shape (Fig. 4a).

The dissolution rate of poly-ACMO was measured using UV–Vis absorbance spectroscopy, monitoring the characteristic absorption peak of poly-ACMO at 317 nm (see Methods). Of all the designs, Design 1 had the fastest release rate (4.07 ± 0.25 mg/min) over ~50 min, due to the unconstrained release from the soluble formulation component in the upper, lower and radial surfaces (Fig. 4b). Top and bottom barriers of insoluble material in Design 2 reduced the dissolution rate to 2.17 ± 0.04 mg/min and extended the dissolution time to over 80 min. Design 3 reduced the release rate further to 0.98 ± 0.04 mg/min, as the outer wall reduced the available surface area for dissolution compared to Designs 1 and 2. Design 4 showed an initial release comparable to that observed from Design 2 (2.17 ± 0.04 mg/min), followed by transition to a significantly lower release rate of 0.70 ± 0.13 mg/min, as the poly-ACMO front moved through the inner insoluble separating wall. The release rates observed for these multimaterial designs (Fig. 4c) are comparable with the dissolution rates from single material prints illustrated in Fig. 2a. For both single material and multimaterial tablets, the dissolution rate is determined by the contact surface area, as expected from the Noyes-Whitney equation (Fig. 2 and Supplementary Information, SI3, Figure S7). Importantly, the design flexibility offered by MM-IJ3DP can provide the additional benefits of complex delivery strategies with pre-designed release times and rates, as well as potential for the delivery of multiple pharmaceutical agents in a single tablet. Further detailed studies are needed to fully explore these potentials. Dissolution of poly-ACMO was accompanied by release of aspirin. High Performance Liquid Chromatography (HPLC) measurements revealed broad mapping of the release of aspirin to the release of poly-ACMO. The first 70 min showed the fastest aspirin release for Design 1, with reduced rates for Designs 2 and 3 and a two-stage release profile for Design 4. Our results demonstrate a high degree of control of the release rate and introduced complexities, such as changes in the release rate and duration of release. Furthermore, it also demonstrates that for rapid evaluation of designs, it is reasonable to use the release of poly-ACMO as a proxy for drug dissolution. This approach to dosage form manufacture demonstrates how, through manipulation of the combination of soluble and non-soluble materials, it may be possible to control the release of an API in a customised manner, not achievable by other methods.

The results achieved here on control of release rates and the timing of release are enabled by the unique capabilities of MM-IJ3DP, and could advance the field of personalised pharmaceutics. The methods and materials developed here overcome the limitations of low production speed and printing resolution in extrusion based AM used to date [41],

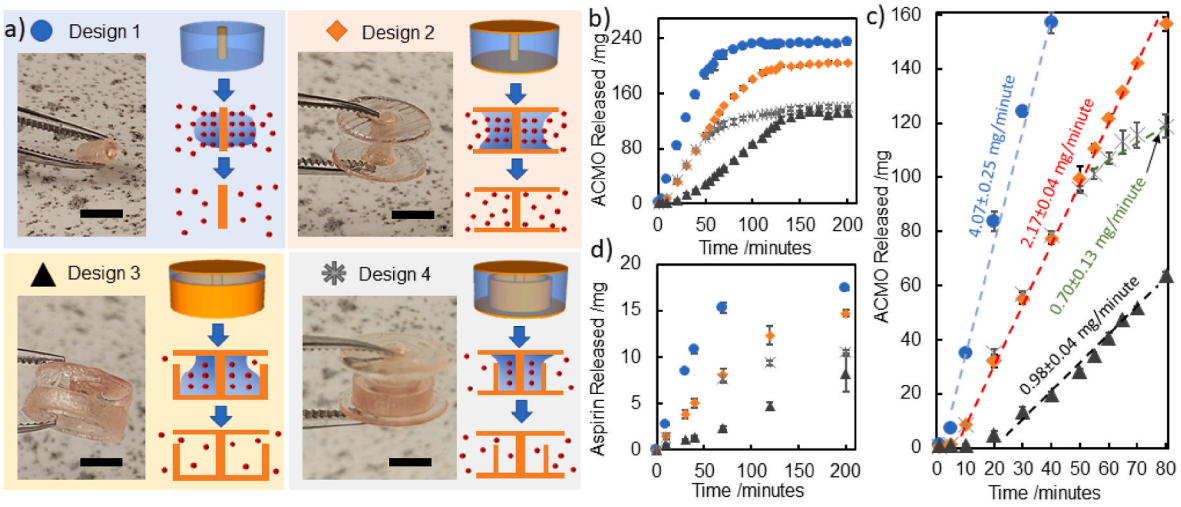

Fig. 4. Tablets with four different release behaviours were designed and printed through MM-IJ3DP process: **a)** Schematic of the four different tablet designs and the photos of the residues after the loaded excipient were fully released, scale bar 4 mm; **b)** Poly-ACMO releasing profile tested by USP II, mean ± standard deviation with $n = 4$; **c)** the linear fitted releasing curve for the first 75 min of the drug releasing from the 4 different designs; **d)** Shows the release profile of aspirin loaded tablets of the four designs measured by HPLC, tested by USP II, mean ± standard deviation with $n = 4$.

and offer opportunities for in-one-batch fabrication of customized structures with complex designs (Figs. 1 and 3). Inkjet-based AM offers 5–10 times higher printing resolution (10–80 μm), compared to extrusion (100–800 μm) [42], however, the availability of suitable functional material inks with different solubility profiles is limited. Structural designs of multimaterial tablets with the ACMO formulation, explored in our work, allow us to achieve release periods of 1.5 h–3 h, which have not been possible with the inkjet-printable excipients used to date, that enable either rapid burst release within seconds [43] or drug out-diffusion release of 4–100 h [19,20,44,45].

Importantly, the MM-IJ3DP utilised in our work, enables unprecedented control of multimaterial design opportunities to enable the control of dosing and release rate without an increase in the overall tablet size. This was demonstrated with examples of four designs of 8 mm diameter tablets (Fig. 4), with the dose defined by the quantity of the soluble component of the structure containing the drug, and where the release rate is governed by the surface area and the time of release of the next dose is controlled by the geometry of the non-soluble component. The experimentally established dependence between the surface area of non-toxic soluble ACMO and the release rate is well described by the Noyes Whitney equation for both single and multimaterial designs (Fig. 2 and Supplementary Information SI3).

3. Conclusion

We demonstrated MM-IJ3DP using a novel formulation of a soluble polymer, poly-ACMO, enabling Noyes–Whitney release rates to be programmed and modulated through digital design and manufacture, for the first time. This advancement represents the foundation for a future of personalised printed polypills exploiting a wide array of release modalities, with release rates easily programmed through their 3D-printed structure. Poly-ACMO is shown to be biocompatible and was used as a model excipient to demonstrate dissolution-mode delivery of aspirin with design-controlled release rates and timed changes of release. Unlike other photo-polymerised excipients, the dissolution behaviour of this formulation makes new opportunities for 3D printed pharmaceutical tablets possible, enabling manufacturers new ‘voxel by voxel’ design freedoms and the capacity to programme the dissolution behaviour of the tablet. This enables enhanced control over drug release profiles, improving patient outlook and therapeutic consistency. The release profile of the drug compound matched that of the excipient dissolution, indicating that future designing and testing of geometries for desired release profiles will be facile and rapid. The opportunities offered by MM-IJ3DP for in-batch manufacturing of different designs, combined with the controlled release of the API demonstrated here, offer realistic opportunities for advanced pharmaceutics manufacturing and personalised medicines.

4. Experimental methods

4.1. Ink preparation and characterization

All chemicals used were purchased from Sigma-Aldrich and used as received. 4-Acryloylmorpholine (ACMO, 97 % contains 1000 ppm monomethyl ether hydroquinone as inhibitor) was prepared as a soluble ink without or with 0, 10, 20, 30 and 40 wt% of aspirin. Tricyclo[5.2.1.0 2,6]decanedimethanol diacrylate (TCDMDA) and Ethylene glycol dicyclopentenyl ether acrylate (EGDPEA) in a 25:75 wt ratio was prepared as the barrier ink. 2,4-Diethyl-9H-thioxanthen-9-one (DETX, 98 %) and Ethyl 4-(dimethylamino)benzoate (EDB, 99 %) were used as type II photoinitiator system and added into the formulation at 3 wt% each. The mixture was stirred at 800 rpm at 40 °C until all the solids fully dissolved (~10 min). The inks were then filtered using a 5 μm PTFE syringe filter and stored at room temperature for 12 h before use. The inks were stored in a vial at room temperature and were stable for a period of at least 8 weeks.

Ink viscosity, μ, was measured using rheometer (Malvern Kinexus Pro) with parallel plate (40 mm) setup at 150 μm sample gap. A shearing rate scan from 10 S^{-1} to 1000 S^{-1} was performed for temperatures of 25, 35, 45, and 55 °C. The surface tension, γ was measured through pendant droplet shape analysis on Kruss Drop Shape Analyser 100S at room temperature (5 replicates). The printing indicator Z, was calculated as:

$$Z = \frac{\sqrt{\rho r \gamma}}{\mu}$$

where ρ is the density of the ink and r=17 μm is the nozzle diameter.

4.2. MM-IJ3DP

The ink printability tests were performed on a Fujifilm Dimatix DMP-2830 material printer. Inks were loaded into 3 pL Dimatix Samba cartridge (17 μm nozzle size) in a dark room and were stored wrapped in foil. Photo-curing was achieved using a UV unit (λ = 365 nm and 600 mW/cm^2) mounted directly on the printhead carriage.

Multi-material printing and tablet batch printing were performed on a PixDRO JETx multi-material printer, using one Spectra SP-128/SE printhead for each ink. Up to 20 mL of each ink was filtered into the printhead reservoirs with UV protection in place to prevent early curing, the printheads were flushed using the ink. UV-triggered pinning and curing of the inks were achieved using the integrated UV unit (LEDZero Solidcure 2, λ = 395 nm, Integration Technology); pinning was performed immediately after deposition of a printed swathe (substrate speed 300 mm/s, lamp height 5 mm, UV intensity 50 %, UV segments 1–7), and curing was performed at the end of each material layer (substrate speed 50 mm/s, lamp height 5 mm, UV intensity 50 %, UV segments 1–7). Printhead temperature, jetting waveform, and printing resolution were determined experimentally (Supplementary Information SI1, Table S1). Layer thickness was determined by printing and measuring specimens composed of 5, 10, and 20 printed layers (Table S2). The nozzle was offset by 17 pixels after each printed layer to reduce surface roughness. The printed structures were stored in a sealed dry environment and had a shelf life of at least 4 weeks.

4.3. Indirect cytotoxicity assay

A PrestoBlue™ assay was used to investigate the indirect cytotoxicity of ACMO on mouse 3T3 fibroblasts (originally sources from the European Collection of Authenticated Cell Cultures (ECACC)). 3T3s cells were grown in Dulbecco’s Modified Eagle’s Medium (DMEM) supplemented with 10 % (*v/v*) fetal bovine serum and 1 % (*v/v*) penicillin/streptomycin antibiotic (final concentration 100 units/mL of penicillin and 100 μg/mL of streptomycin) within a humidified environment at 37 °C, 5 % CO_2 in air. The sub-cultured cells were harvested, suspended in a culture medium, and then seeded at a density of 20,000 cells per well in 48 well plates. The cells were incubated at 37 °C and 5 % CO_2 in air for 24 h. The culture medium in well-plates was removed, and the cells were treated with a culture medium containing different concentrations of printed ACMO (0.001, 0.01, 0.1, and 1 % (*w/v*)), culture medium alone (as positive controls), and 10 % (*v/v*) DMSO (as negative control). Samples at concentrations of 1 % (*w/v*) were centrifuged at 12,000 rpm for 30 min to separate the undissolved printed ACMO in culture medium. Prior to use, the printed poly-ACMO was sterilized under UV light using UVP CL-1000 UV crosslinker for 30 min, and the solution was filtered using a 0.22 μm syringe filter.

Following the required exposure time (1, 6, and 24 h), the medium was aspirated, and the cells washed with phosphate-buffered saline (PBS pH7.4). Presto blue solution, 10 % (*v/v*) in DMEM was then added (200 μL) to the cells and incubated for 30 min at 37 °C and 5 % CO_2 in air (covered with aluminium foil to avoid exposure to light). The 100 μL of incubated PrestoBlue™ solution from 48 well-plates was transferred to 96 well-plates, and fluorescence measured using a Tecan Infinite 200

microplate reader (TECAN, Switzerland) at excitation 560 nm and emission 590 nm. The cell viability was presented as a percentage relative to the positive control at the respective timepoint. The samples were prepared in quadruplicates to calculate the mean values and standard deviation.

4.4. Dissolution and drug release tests

A Copley's Dissolution Test Dis8000 (Nottingham, UK) was utilised to determine the dissolution release of poly-ACMO. Samples were loaded into 40 mesh (USP) baskets, covered in 500 mL of 10 mM phosphate buffer (pH 7.4 at 25 °C) and incubated at 37.0 ± 0.1 °C under stirring at 50 rpm. Samples (5 mL) were collected at regular intervals and filtered via a 0.45 μm MF-Millipore membrane filter (MILLEX HA). An equivalent amount of fresh buffer was reintroduced after each sampling to maintain the buffer level constant. All dissolution tests were conducted in triplicate. The amount of excipient dissolved into the medium was determined using UV–visible spectrophotometry. Samples (300 μL) were loaded into a quartz well-plate (Hellma, Essex, UK) and analysed using a Spark Microplate Reader (Tecan Trading AG Männedorf, Switzerland) UV–vis spectrophotometer. The analysis was carried out in the 200–500 nm range using characteristic absorbance peak at $\lambda_{max} = 317$ nm to quantify dissolved poly-ACMO. Samples that surpassed the detection limits during testing were diluted in 1:1 ratio using a 10 mM phosphate buffer before conducting a repeat test to ensure the accuracy of the results. The amount of aspirin released from the formulations was determined on an Agilent Technologies 1200 Series HPLC system using an ACE Excel 5C18 column (250 × 4.6 mm id) maintained at 25 °C. A mobile phase of 72:28 (*v/v*) ratio of 0.7 M acetic acid in water: methanol was employed at a flow rate of 1 mL/min. The eluent was monitored using a variable wavelength detector at 275 nm with a peak eluting at a retention time of 16 min.

4.5. Raman spectroscopy

Micro Raman spectroscopy was performed using a HORIBA LabRAM HR Raman microscope. Spectra were acquired using a 785 nm laser (20 mW power), a 50 × objective and a 300 μm confocal pinhole. A 300 lines mm^{-1} rotatable diffraction grating along a path length of 800 mm was used. Spectra were detected using a Synapse CCD detector (1024 pixels). For *xy*-mapping, spectra were acquired within the range 490–1830 cm^{-1} (one spectral window) over an area of 6600 × 6600 μm (50 μm steps). The DuoScan functionality was employed to control the laser spot size and confer a spatial resolution of ~50 × 50 × 20 μm in the *x*, *y* and *z* dimensions, respectively. To account for differences in height for the poly-ACMO-only and poly-ACMO with aspirin areas, a single *xy*-plane was fixed at 25 μm below the focal plane of the poly-ACMO with aspirin areas (under focus) and 25 μm above the focal plane of the poly-ACMO-only area (over focus). Spectra were baseline corrected using a third order polynomial model. False colour images were created by fitting the component spectra obtained from an ACMO-only reference print (red), an ACMO-aspirin print (green) and the silicon substrate (blue) using classic least squares (CLS) regression analysis. CLS scores were normalized to 100 %.

4.6. Differential Scanning Calorimetry (DSC)

The printed specimens of poly-ACMO and 30 % (*w/w*) aspirin-poly-ACMO were analysed using Perkin Elmer DSC 8000 under nitrogen, scanning between 40 °C and 200 °C at 10 °C/min. The glass transition temperature was recorded as the middle of the sloped region.

4.7. X-ray diffraction (XRD)

D8 Advance DaVinci (Bruker, Billerica, MA, USA) Cu Kα radiation (40 kV and 40 mA) and an Ni filter was used to perform the pXRD analysis. The scanning speed was set to 0.02° 2θ s^{-1} with the divergence slit at 0.3°, the anti-scatter slit at 5.2 mm. Spectra were collected in the 3 to 70 2θ range at room temperature. Table samples were loaded onto PMMA sample holders (8.5 mm height and 25 mm diameter) from Bruker (Billerica, MA, USA) and analysed without further manipulation. Powder sample (Aspirin) was added onto the holder, pressed and the top surface smoothed using a glass slide, the process was repeated until a smooth surface was achieved.

4.8. Friability test

To test the friability of the printed samples a FRV 2000 (Copley, Nottingham, UK) was used with a standard 300 mm diameter drum attachment. Ten tablets were dedusted, weighed and loaded into the drum. The rotational speed was set to a constant 25 rpm. All samples were removed, dusted, weighed and reloaded into the drum every 25 revolutions for a total of 200 overall revolutions. Weight measurements were carried out using a high precision scale (Kern ALS Analytical Balance, Balingen, Germany).

4.9. Gel permeation chromatography (GPC)

Aqueous GPC was performed on an Agilent 1200 system fitted with an RI detector, Agilent two PL aquagel-OH column and one aquagel guard column eluted with 0.1 M $NaNO_3$ eluent. Molecular weight (Mn) and polydispersity (Đ) were calculated according to PEG narrow standards (1500–0.105 kDa) using Agilent EasyVial calibrants fitted with a cubic function to correlate retention time and molar mass. Polymer samples were made by dissolving 3 mg/mL pure polymer in 0.1 M $NaNO_3$. 50 μL samples were injected and eluted at 1 mL/min for 30 min.

4.10. Attenuated total reflection infrared (ATR-IR) spectroscopy

A PerkinElmer UATR IR was used. The spectra for each set of samples were normalized to the acrylate carboxyl group peak at 1726 cm^{-1}. Characteristic peaks at 950 cm^{-1} (γ C═C) and 790 cm^{-1} (=CH) were used to analyse the level of monomer conversion [33].

4.11. Nuclear magnetic resonance (NMR) spectroscopy

^1H NMR spectra were recorded at 25 °C using Bruker AV400 and AV3400 spectrometers (400 MHz). Samples were dissolved in deuterated solvent $CDCl_3$ to which chemical shifts are referenced (residual chloroform at 7.26 ppm). The integrated intensities of the morpholine $–CH_2$ peak (centred at 3.64 ppm, 8 protons) were compared with the benzene peak of the aspirin (8.09 ppm, 7.60 ppm, 7.36 ppm and 7.13 ppm, each represents one proton). MestReNova 14.2.1 copyright 2021 (Mestrelab Research S. L.) was used for analysing the spectra.

CRediT authorship contribution statement

Geoffrey Rivers: Writing – review & editing, Writing – original draft, Formal analysis, Conceptualization. **Anna Lion:** Methodology, Formal analysis, Data curation. **Nur Rofiqoh Eviana Putri:** Methodology, Data curation. **Graham A. Rance:** Writing – original draft, Methodology, Formal analysis, Data curation, Conceptualization. **Cara Moloney:** Methodology, Formal analysis, Data curation. **Vincenzo Taresco:** Methodology, Formal analysis, Data curation, Conceptualization. **Valentina Cuzzucoli Crucitti:** Methodology, Formal analysis, Data curation, Conceptualization. **Hannah Constantin:** Methodology, Data curation. **Maria Inês Evangelista Barreiros:** Methodology, Data curation. **Laura Ruiz Cantu:** Methodology, Conceptualization. **Christopher J. Tuck:** Supervision, Funding acquisition. **Felicity R.A.J. Rose:** Supervision, Resources, Methodology, Funding acquisition, Formal analysis, Data curation, Conceptualization. **Richard J.M. Hague:** Supervision, Resources, Funding acquisition. **Clive J. Roberts:**

Methodology, Conceptualization. **Lyudmila Turyanska:** Writing – review & editing, Writing – original draft, Supervision, Methodology, Investigation, Formal analysis, Data curation, Conceptualization. **Ricky D. Wildman:** Writing – review & editing, Writing – original draft, Supervision, Resources, Methodology, Funding acquisition, Formal analysis, Data curation, Conceptualization. **Yinfeng He:** Writing – review & editing, Writing – original draft, Supervision, Methodology, Formal analysis, Data curation, Conceptualization.

Declaration of competing interest

The authors declare that they have no known competing financial interests or personal relationships that could have appeared to influence the work reported in this paper.

Data availability

The link to the data has been shared in the maintext

Acknowledgements

This work was funded by the Engineering and Physical Sciences Research Council [grant numbers EP/P031684/1 and EP/W017032/1]. The authors acknowledge access to facilities at the Nanoscale and Microscale Research Centre (nmRC) of the University of Nottingham.

Appendix A. Supplementary data

Supplementary data to this article can be found online at https://doi.org/10.1016/j.mtadv.2024.100493.

References

[1] I.P. Žitnik, D. Zerne, I. Mancini, L. Simi, M. Pazzagli, C. Di Resta, H. Podgornik, B. R. Lampret, K.T. Podkrajšek, C. Sipeky, R. Van Schaik, I. Brandslund, P. Vermeersch, M. Schwab, J. Marc, Clin. Chem. Lab. Med. 56 (2018) 1981.
[2] M.A. Hamburg, F.S. Collins, N. Engl. J. Med. 363 (2010) 301.
[3] Y. Yamamoto, N. Kanayama, Y. Nakayama, N. Matsushima, J. Personalized Med. 12 (2022) 444.
[4] H. Kang, S. Wang, C. Li, K. Wang, J. Sun, Langmuir 40 (12) (2024) 6571–6581.
[5] M. Ma, R. Sun, H. Kang, S. Wang, P. Jia, Y. Song, J. Sun, Colloids Surf. B Biointerfaces 231 (2023) 113571.
[6] M. Ma, R. Sun, S. Li, H. Kang, S. Wang, F. Chu, J. Sun, Sensor Actuat A-Phys 351 (2023) 114161.
[7] P. Robles-Martinez, X. Xu, S.J. Trenfield, A. Awad, A. Goyanes, R. Telford, A. W. Basit, S. Gaisford, Pharmaceutics 11 (6) (2019), https://doi.org/10.3390/PHARMACEUTICS11060274.
[8] H. Windolf, R. Chamberlain, J. Breitkreutz, J. Quodbach, Pharmaceutics 14 (2022) 931.
[9] S.A. Khaled, J.C. Burley, M.R. Alexander, J. Yang, C.J. Roberts, J. Contr. Release 217 (2015) 308.
[10] G. Chen, Y. Xu, P.C.L. Kwok, L. Kang, Addit. Manuf. 34 (2020) 101209.
[11] S.K. Patel, M. Khoder, M. Peak, M.A. Alhnan, Adv. Drug Deliv. Rev. 174 (2021) 369.
[12] G. Auriemma, C. Tommasino, G. Falcone, T. Esposito, C. Sardo, R.P. Aquino, Mol. 27 (2022) 2784, 2022, 27, 2784.
[13] H. Ragelle, S. Rahimian, E.A. Guzzi, P.D. Westenskow, M.W. Tibbitt, G. Schwach, R. Langer, Adv. Drug Deliv. Rev. 178 (2021) 113990.
[14] A. Elkaseer, K.J. Chen, J.C. Janhsen, O. Refle, V. Hagenmeyer, S.G. Scholz, Addit. Manuf. 60 (2022) 103270.
[15] E. Saleh, F. Zhang, Y. He, J. Vaithilingam, J.L. Fernandez, R. Wildman, I. Ashcroft, R. Hague, P. Dickens, C. Tuck, Adv. Mater. Technol. 2 (10) (2017) 1700134.
[16] H. Kansara, M. Liu, Y. He, W. Tan, J. Mech. Phys. Solid. 180 (2023) 105382.
[17] Y. He, M. Abdi, G.F. Trindade, B. Begines, J. Dubern, E. Prina, A.L. Hook, G.Y. H. Choong, J. Ledesma, C.J. Tuck, E.R.A.J. Rose, R.J.M. Hague, C.J. Robert, D.S. A. De Focatiis, I.A. Ashcroft, P. Williams, D.J. Irvine, M.R. Alexander, R. D. Wildman, Adv. Sci. 8 (15) (2021) 2100249.
[18] S. Borandeh, B. van Bochove, A. Teotia, J. Seppälä, Adv. Drug Deliv. Rev. 173 (2021) 349.
[19] E.A. Clark, M.R. Alexander, D.J. Irvine, C.J. Roberts, M.J. Wallace, J. Yoo, R. D. Wildman, Int. J. Pharm. 578 (2020) 118805.
[20] Y. He, R. Foralosso, G.F. Trindade, A. Ilchev, L. Ruiz-Cantu, E.A. Clark, S. Khaled, R.J.M. Hague, C.J. Tuck, F.R.A.J. Rose, Adv. Ther. 3 (2020) 1900187.
[21] J. van der Merwe, J. Steenekamp, D. Steyn, J. Hamman, Pharm. Times 12 (2020) 393, 2020, 12, 393.
[22] C.E. Beneke, A.M. Viljoen, J.H. Hamman, Mol 14 (2009) 2602–2620, 2009, 14, 2602.
[23] G. Majid Khan, J.B. Zhu, J. Contr. Release 57 (1999) 197.
[24] A. Wahab, G.M. Khan, M. Akhlaq, N.R. Khan, A. Hussain, M.F. Khan, H. Khan, A. Wahab, Pharmazie 66 (2011) 677.
[25] P. K. Parmar, S. G. Rao, A. K. Bansal, https://doi-org.nottingham.idm.oclc.org/10.1080/17425247.2021.1873946 2021, 18, 907..
[26] S. Wilfert, A. Iturmendi, W. Schoefberger, K. Kryeziu, P. Heffeter, W. Berger, O. Brüggemann, I. Teasdale, J. Polym. Sci. Part A Polym. Chem. 52 (2014) 287.
[27] M.J. Choi, M.R. Woo, H.G. Choi, S.G. Jin, Int. J. Mol. Sci. 23 (2022) 9491, 2022, 23, 9491.
[28] B. Jadach, W. Świetlik, A. Froelich, J. Pharmaceut. Sci. 111 (2022) 1250.
[29] K.A. Farley, M.R.M. Koos, Y. Che, R. Horst, C. Limberakis, J. Bellenger, R. Lira, L. F. Gil-Silva, R.R. Gil, Angew. Chem., Int. Ed. 60 (2021) 26314.
[30] I. Seoane-Viaño, S.J. Trenfield, A.W. Basit, A. Goyanes, Adv. Drug Deliv. Rev. 174 (2021) 553–575.
[31] C. Gyles, Can. Vet. J. 60 (10) (2019) 1033.
[32] Z. Abousalman-Rezvani, H. Roghani-Mamaqani, H. Riazi, O. Abousalman, Rezvani Polym. Chem. 13 (42) (2022) 5940–5964.
[33] L. Wang, X. Liu, Int. J. Environ. Res. Publ. Health 16 (12) (2019) 2153.
[34] A. Dokoumetzidis, V. Papadopoulou, P. Macheras, Pharm. Res. (N. Y.) 23 (2006) 256–261.
[35] Z. Gao, J. Pharmaceut. Sci. 100 (11) (2011) 4934–4942.
[36] R.E. Osterberg, N.A. See, Int. J. Toxicol. 22 (5) (2003) 377–380.
[37] M.M. Mau, S. Sarker, B.S. Terry, Prog. Biomed. Eng. 3 (2021) 042001.
[38] M.N. Siddiqui, G. Garg, P.K. Sharma, Int. J. Pharmaceut. Sci. Rev. Res. 4 (2) (2010) 87–96.
[39] P. Chakma, S.M. Zeitler, F. Baum, J. Yu, W. Shindy, L.D. Pozzo, M.R. Golder, Angew. Chem. Int. Ed. 135 (2) (2022) e202215733.
[40] D. Siefker, R.A. Chan, M. Zhang, J. Nho, D. Zhang, Macromolecules 55 (2022) 2509–2516.
[41] M. Salmi, Materials 14 (1) (2021) 191.
[42] Q. Ge, Z. Li, K. Kowsari, W. Zhang, X. He, J. Zhou, N.X. Fang, Int. J. Extrem. Manuf. 2 (2) (2020) 022004.
[43] L. Krueger, J.A. Miles, K.J. Steadman, T. Kumeria, C.R. Freeman, A. Popat, Med. J. Aust. 216 (2) (2022) 64–67.
[44] M. Kyobula, A. Adedeji, M.R. Alexander, E. Saleh, R. Wildman, I. Ashcroft, P. R. Gellert, C.J. Roberts, J. Contr. Release 261 (2017) 207–215.
[45] A. Lion, R.D. Wildman, M.R. Alexander, C.J. Roberts, Pharm. Times 13 (10) (2021) 1679.